Available online at www.sciencedirect.com
SCIENCE DIRECT
Fuel 85 (2006) 1729–1742
FUEL
www.fuelfirst.com

NO_x emission characteristics of counterflow syngas diffusion flames with airstream dilution

Daniel E. Giles, Sibendu Som, Suresh K. Aggarwal *

Department of Mechanical and Industrial Engineering, University of Illinois at Chicago, 842 West Taylor Street, Chicago, IL 60607-7022, USA

Received 7 October 2005; received in revised form 27 January 2006; accepted 30 January 2006
Available online 9 March 2006

Abstract

Syngas is produced through a gasification process using variety of fossil fuels, including coal, biomass, organic waste, and refinery residual. Although, its composition may vary significantly, it generally contains CO and H_2 as the dominant fuel components with varying amount of methane and diluents. Due to its wide flexibility in fuel sources and superior pollutants characteristics, the syngas is being recognized as a viable energy source worldwide, particularly for stationary power generation. There are, however, gaps in the fundamental understanding of syngas combustion and emissions, as most previous research has focused on flames burning individual fuel components such as H_2 and CH_4, rather than syngas mixtures. This paper reports a numerical investigation on the effects of syngas composition and diluents on the structure and emission characteristics of syngas nonpremixed flames. The counterflow syngas flames are simulated using two representative syngas mixtures, 50%H_2/50%CO and 45%H_2/45%CO/10%CH_4 by volume, and three diluents, N_2, H_2O, and CO_2. The effectiveness of these diluents is characterized in terms of their ability to reduce NO_x in syngas flames. Results indicate that syngas nonpremixed flames are characterized by relatively high temperatures and high NO_x concentrations and emission indices. The presence of methane in syngas decreases the peak flame temperature, but increases the formation of prompt NO significantly. Consequently, while the total NO formed is predominantly due to the thermal mechanism for the 50%H_2/50%CO mixture, it is due to the prompt mechanism for the 45%H_2/45%CO/10%CH_4 mixture. For both mixtures, CO_2 and H_2O are more effective than N_2 in reducing NO_x in syngas flames. H_2O is the most effective diluent on a mass basis, while CO_2 is more effective than N_2. The effectiveness of H_2O is due to its high specific heat that decreases the thermal NO, and its ability to significantly reduce the concentration of CH radicals, which decreases the prompt NO. The presence of methane in syngas reduces the effectiveness of all three diluents.

Keywords: Syngas fuel; NO_x emissions; Effect of diluents

1. Introduction

Syngas or synthetic gas is formed through the gasification process, and can be produced from virtually any fossil fuel, including coal, biomass, organic waste, and refinery residual [1,2]. As the world energy demand and environmental concern continue to grow, syngas is expected to play an important role in future energy production. It represents a viable energy source, particularly for stationary power generation, since it allows for a wide flexibility in fossil fuel sources, and since most of the harmful contaminants and pollutants can be removed in the post-gasification process prior to combustion. Moreover, improvements in gas turbine efficiency and reliability have made syngas a viable fuel for electric power generation using integrated gasification combined cycle (IGCC) systems [3]. In spite of many advantages of syngas, however, its environmental feasibility needs to be fully established. In particular, NO_x emissions from syngas combustion must comply with the current and future emission regulations. For instance, a recent DOE initiative aims at reducing NO_x emissions from syngas combustion systems to less than 3 ppm, well below the current US regulations [3]. This provides a major motivation for fundamental research focusing on syngas combustion and emissions.

There is an extensive body of literature dealing with the structure and emission characteristics of counterflow diffusion flames. However, most of these studies have focused on the combustion of individual syngas components, such as methane [4,5] and hydrogen fuels [6–8], rather than on syngas mixtures. Similarly, previous studies dealing with the effects of diluents on emissions have generally focused on the emission characteristics of CH_4–air and H_2–air flames, rather than of

* Corresponding author. Tel.: +1 312 996 2235; fax: +1 312 413 0441.
E-mail address: ska@uic.edu (S.K. Aggarwal).

0016-2361/$ - see front matter © 2006 Elsevier Ltd. All rights reserved.
doi:10.1016/j.fuel.2006.01.027

syngas flames. Li et al. [4] conducted an experimental and numerical study on the effects of air stream dilution using various agents (N_2, H_2O, CO_2, and Ar) on NO_x emission from CH_4–air counterflow flames. On a mass basis, the effectiveness of various diluents in reducing NO_x emission was found to rank in the order: $H_2O > CO_2 > N_2 > Ar$. The higher effectiveness of H_2O was due to its higher heat capacity that reduces the flame temperature and thereby the thermal NO, and its ability to reduce the concentration of CH radicals that reduces the prompt NO. Zhao et al. [5] examined numerically the effects of steam addition on NO_x formation in methane–air diffusion flames, and observed a 17% reduction in NO_x emission index with a 5% mass addition while maintaining the same flame temperature. Rortveit et al. [6] reported experimental and numerical results on the effects of various diluents in the fuel stream on NO_x emissions from H_2–air nonpremixed and partially premixed flames. On a mole basis, CO_2 was found to be a more effective diluent compared to N_2 in reducing both the flame temperature and NO_x concentration in these flames. Park et al. [7] also investigated the effect of steam addition on NO formation in H_2–O_2–N_2 diffusion flames. Naha et al. [9,10] reported a numerical investigation on the effects of blending hydrogen with different fuels (methane and *n*-heptane) on NO_x emissions in counterflow nonpremixed and partially premixed flames. They observed that hydrogen blending has a more favorable effect on NO_x emissions in *n*-heptane flames compared to that in methane flames. This was attributed to a dramatic reduction in prompt NO due to hydrogen addition in *n*-heptane flames.

Some previous studies have focused on the combustion and emission characteristics of syngas mixtures. Allen et al. [11] studied the oxidation chemistry of $CO/H_2O/N_2$ mixtures. Drake and Blint [12] numerically investigated the effect of stretch on thermal NO in laminar, counterflow $CO/H_2/N_2$ diffusion flames, and observed that NO concentration decreases dramatically as the flame stretch is increased. Chung and Williams [13] analyzed the structure and extinction of a $CO/H_2/N_2$ diffusion flame using an asymptotic approach. Fotache et al. [14] examined experimentally and numerically the ignition characteristics of a $CO/H_2/N_2$ mixture using heated air in a counterflow configuration. Charlston-Goch et al. [15] reported measurement and computation of NO concentrations in premixed $CO/H_2/CH_4$/air flames at high pressures. Rumminger and Linteris [16] reported an experimental and numerical investigation on the burning velocity of premixed $CO/H_2/O_2/N_2$ flames with the objective of assessing the fire inhibition characteristics of iron pentacarbonyl. Natarajan et al. [17] also reported measurement and computation of laminar flame speeds of $H_2/CO/CO_2$ mixtures over a range of fuel compositions, lean equivalence ratios, and reactant preheat temperatures. Alavandi and Agrawal [18] investigated experimentally the lean premixed combustion of $CO/H_2/CH_4$/air mixture, and observed that at a given flame temperature, the presence of CH_4 in a CO–H_2 mixture increases CO and NO_x emissions.

The syngas composition varies widely depending upon the fossil fuel source, gasification process, and post-gasification treatment. In addition, the type and amount of diluents present during syngas combustion can vary significantly. These variations are well illustrated in Table 1 taken from Ref. [19], which lists the composition of syngas fuel and the various diluents used in gas turbine power generation facilities in different regions of the world. Our literature review indicates that while the combustion and emission characteristics of individual syngas components, such as hydrogen and methane, have been extensively investigated, the corresponding research dealing with the combustion of syngas mixtures has been relatively sparse. Consequently, there is a gap in our fundamental understanding of the combustion and emission characteristics of various syngas mixtures. Further experimental and numerical investigations are needed to characterize the detailed structure of syngas flames, and the effects of various diluents on emissions from these flames.

Motivated by this consideration, we report herein a numerical investigation of syngas nonpremixed flames in a counterflow configuration, and characterize the effects of various diluents on NO_x emissions in these flames. The counterflow configuration is employed so that more comprehensive chemistry and transport models can be used for a detailed investigation of the structure and emission characteristics of syngas flames. The syngas flames are simulated using two representative syngas mixtures containing CO, H_2, and CH_4, one containing 50% H_2 and 50% CO by volume and the other 45% H_2, 45% CO, and 10% CH_4 by volume. The selection of these two mixtures is based on the composition of syngas mixtures used in various power generation systems listed in Table 1. As indicated in this table, while the syngas composition may vary significantly, CO and H_2 represent the dominant components of most syngas mixtures with varying amounts of methane and diluents. The average syngas composition computed using values from this table are shown in Table 2. Based on these average values and standard deviation, the two syngas mixtures considered in the present study are also shown in this table. The three commonly used diluents used during syngas combustion include N_2, H_2O, and CO_2. Although one or more of diluents may be present or introduced into the syngas mixture during the gasification and refining processes, the present study considers the effects of adding these diluents in the oxidizer stream. This is motivated by the consideration that in syngas combustors used in IGCC systems, diluents are introduced directly into the combustor as opposed to premixing them with syngas prior to injection. A detailed parametric study is performed to characterize the effects of syngas composition and three diluents on the syngas flame structure and NO_x emissions.

2. The numerical model

A schematic of the syngas nonpremixed flame simulated in a counterflow configuration is shown in Fig. 1. This relatively simple configuration facilitates a detailed analysis of the effects of syngas composition and various diluents on the flame structure and the relative contributions of thermal and prompt NO mechanisms for a wide range of conditions. In IGCC power generation systems, the energy is delivered through controlled combustion of syngas in a gas turbine. In

Table 1
Major fuel components and diluents (%volume) in syngas mixtures used in various gas turbine power generation facilities

Syngas	PSI	Tampa	El Dorado	Pernis	Sierra Pacific	ILVA	Schwarze Pumpe	Sarlux	Fife	Exxon Singapore	Motiva Delaware	PIEMSA	Tonghua
H_2	24.8	37.2	35.4	34.4	14.5	8.6	61.9	22.7	34.4	44.5	32.00	42.30	10.3
COPOLYMERS/TERPOLYMERS	39.5	46.6	45.0	35.1	23.6	26.2	26.2	30.6	55.4	35.4	49.50	47.77	22.3
CH_4	1.5	0.1	0.0	0.3	1.3	8.2	6.9	0.2	5.1	0.5	0.10	0.08	3.8
CO_2	9.3	13.3	17.1	30.0	5.6	14.0	2.8	5.6	1.6	17.9	15.80	8.01	14.5
$N_2 + Ar$	2.3	2.5	2.1	0.2	49.3	42.5	1.8	1.1	3.1	1.4	2.15	2.05	48.2
H_2O	22.7	0.3	0.4	–	5.7	–	–	39.8	–	0.1	0.44	0.15	0.9
LHV (Btu/ft^3)	209	253	242	210	128	183	317	163	319	241	248	270.4	134.6
LHV (kJ/m^3)	8224	9962	9528	8274	5024	7191	12492	6403	12568	9477	9768	10655	5304
T_{fuel} F/C	570/300	700/371	250/121	200/98	1000/538	400/204	100/38	392/200	100/38	350/177	570/299	338/170	–
H_2/CO ratio	0.63	0.8	0.79	0.98	0.61	0.33	2.36	0.74	0.62	1.26	0.65	0.89	0.46
Diluent	Steam	N_2	N_2/steam	Steam	Steam	–	Steam	Moisture	H_2O	Steam	H_2O/N	N_2	n/a
Equivalent LHV (Btu/ft^3)	150	118	113[a]	198	110	–	200	–	–[a]	116	150	129	134.6
Equivalent LHV (kJ/m^3)	5910	4649	4452	7801	4334	–	7880	–	–	4600	5910	5083	5304

[a] Always co-fired with 50% natural gas.

Table 2
Average syngas composition and amount of major diluents (vol%) corresponding to syngas mixtures listed in Table 1

Syngas constituent	Average (vol%)	Standard deviation (vol%)
H_2	31.0	14.9
CO	37.2	11.0
CH_4	2.2	2.9
CO_2	12.0	7.7
N_2+Ar	12.2	19.7
H_2O	7.8	14.1
Flame A	50% H_2/50% CO (by volume)	
Flame B	45% H_2/45% CO/10% CH_4	

Compositions of two syngas mixtures considered in the present study are listed.

such systems, diluents are injected into the combustor directly as opposed to premixing them with syngas prior to injection. This allows the fuel control valves to be reduced in size, and the diluent and syngas source feeds to be held at different pressures [9]. Moreover, since the syngas is injected nonpremixed in a gaseous form and quickly ignited within the combustor, fuel–air premixing prior to combustion is assumed to be small, and neglected in this study. From a counterflow flame perspective, this implies the injection of nonpremixed syngas from the fuel nozzle and that of diluted air from the oxidizer nozzle, as shown in Fig. 1.

Simulations of nonpremixed syngas flames are performed using the OPPDIF code [20] with the CHEMKIN package [21]. The OPPDIF code is written in FORTRAN, and used for computing the flow field in a counterflow configuration. An optically thin radiation model is used to account for the radiation heat loss [22]. The temperature of both the fuel and oxidizer streams is taken as 300 K. The velocities of the fuel and oxidizer streams are chosen to conform to the global strain rate

$$a_s = \frac{2|V_O|}{L}\left(1+\frac{|V_F|\sqrt{\rho_F}}{|V_O|\sqrt{\rho_O}}\right) \quad (1)$$

and to satisfy the momentum balance

$$\rho_O V_O^2 = \rho_F V_F^2 \quad (2)$$

here V and ρ represent the velocity and density, respectively, with the subscripts 'O' and 'F' indicating the oxidizer and fuel streams, respectively, and L is the separation distance between the two nozzles, and is taken as 1.27 cm. Using

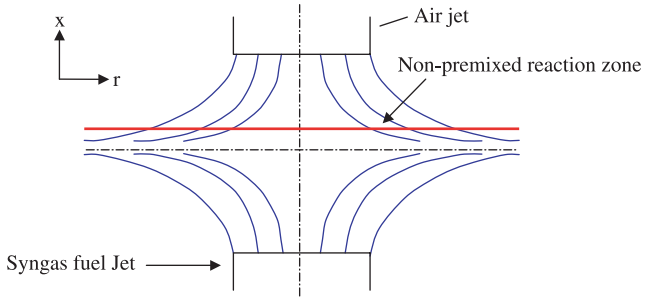

Fig. 1. Schematic of the counterflow nonpremixed flame simulated in the present study.

these two equations, the fuel and air stream velocities can be computed for a given strain rate a_s. The plug flow boundary conditions are used to specify the fuel and air stream velocities at the respective boundaries. Boundary conditions for the species conservation equations require the specification of species mole fractions at the two boundaries. The two syngas mixtures considered in the present study are listed in Table 2. The oxidizer composition is provided by specifying the mole fraction of a given diluent, with the other species being air containing 79% oxygen and 21% nitrogen by volume.

The syngas oxidation chemistry is modeled by using the GRI Mech-3.0 mechanism [23] that involves 53 species and 325 reactions. This is based on the consideration that CO and H_2 represent the dominant components of most syngas fuels, and the oxidation chemistries of these two species are well represented in this mechanism. The GRI 3.0 mechanism and its earlier versions have been extensively validated in previous studies [24–26] using a variety of configurations including perfectly stirred reactors, autoignition and shock-tube ignition delay times, extinction limits, laminar flame speeds, and nonpremixed and partially premixed methane flames.

Since, no experimental data are available for syngas flames, we performed additional validation studies using the available measurements of the flame structure and NO_x profiles in methane–air flames. Fig. 2 presents a comparison of the measured and predicted NO profiles for four different methane–air flames. The first three cases are for partially premixed flames established at a strain rate of $a_s = 20\ s^{-1}$ and at fuel stream equivalence ratio of $\phi = 1.45$, 1.6, and 2.0 [27,28], while the fourth one is for a nonpremixed flame established at a strain rate of $a_s = 162\ s^{-1}$ [29]. It is important to note that there was a good agreement (not shown) between the predicted and measure flame structures in terms of temperature and major species profiles (CH_4, O_2, CO_2, N_2, H_2 and CO). However, the predicted and measured NO profiles indicate that the GRI 3.0 mechanism overpredicts NO mole fractions for fuel rich mixtures (for $\phi \geq 1.6$). This is consistent with the results reported in previous investigations [4,25,28], which have attributed this discrepancy to an overprediction of CH concentration, and thereby of prompt NO by this mechanism. In spite of such discrepancy, the use of this mechanism for the present study is justified by the consideration that no other validated mechanisms are available for syngas flames due to the lack of experimental data, and that GRI 3.0 mechanism and its earlier versions have been extensively used to model flames burning methane and other hydrocarbon fuels such as ethylene and acetylene. In this context, our results pertaining to the effects of syngas composition and diluents on NO_x emissions should be considered qualitative.

3. Results

3.1. Structure and emission characteristics of syngas flames

Two representative syngas mixtures considered in the present investigation are listed in Table 2. The flames

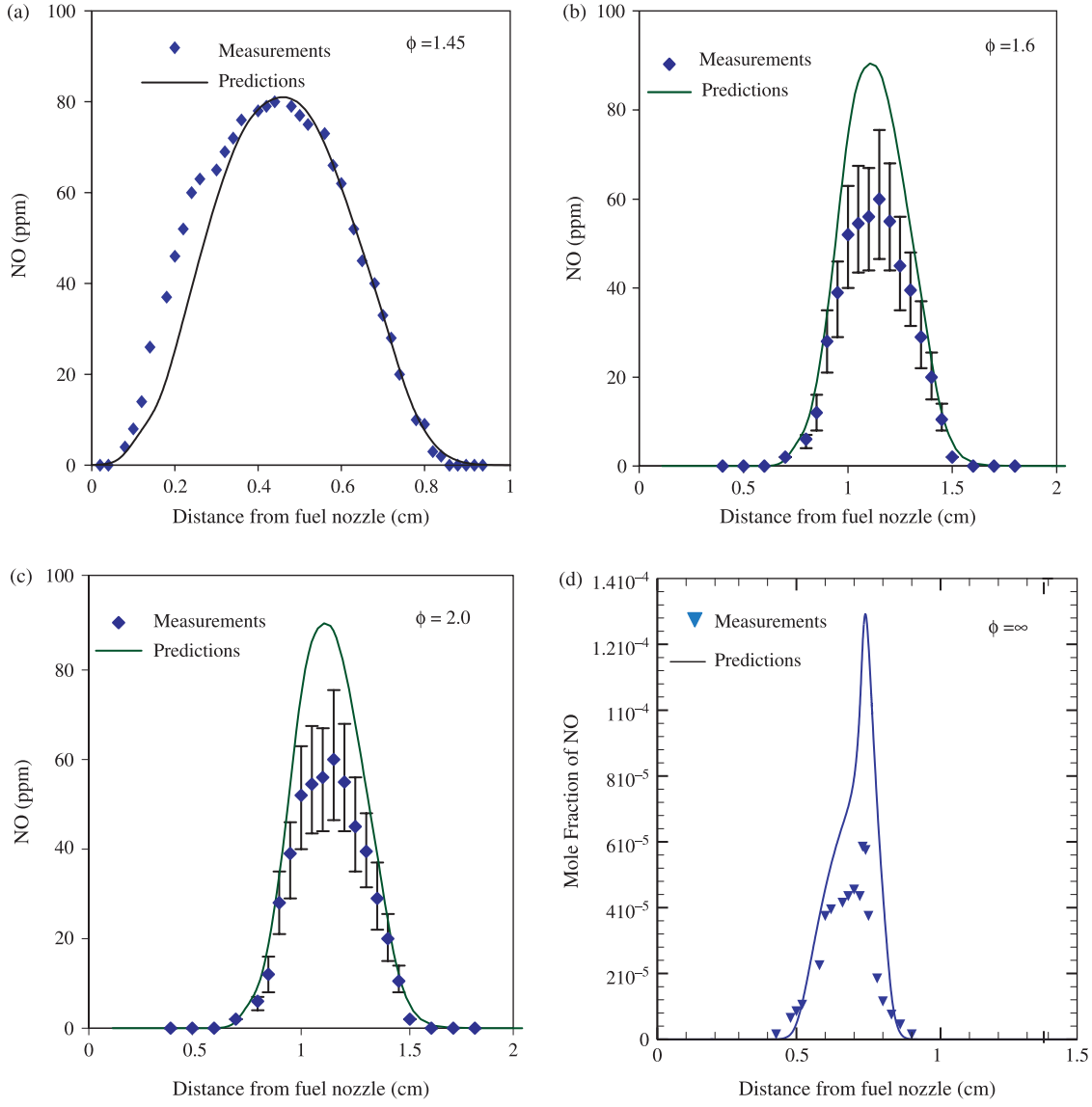

Fig. 2. Comparison of the predicted and measured NO mole fraction profiles for four methane–air flames established at different strain rates and equivalence ratios.

simulated using these two mixtures are designated as flames A and B, respectively. Since, a major focus of this study is to characterize the effectiveness of various diluents by introducing them in the air stream, the syngas is assumed to contain only H_2, CO, and CH_4 fuel species. Moreover, a fixed strain rate of $a_s = 100\ s^{-1}$ is considered in order to focus on characterizing the effectiveness of various diluents on NO_x formation in syngas flames. Since, the amount of thermal NO formed is strongly influenced by the residence time [30], the effect of strain rate will be examined in a future investigation.

Figs. 3 and 4 present the structures of flames A and B, respectively, in terms of the temperature, axial velocity, and species mole fraction profiles. Both the flames are established at a strain rate of $a_s = 100\ s^{-1}$. The global structures of these two flames are similar. As syngas fuel species are transported to and consumed in the nonpremixed reaction zone, the temperature and mole fractions of the major product species (H_2O and CO_2) increase. The reaction zone, located on the oxidizer side of the stagnation plane, is characterized by the peaks in the mole fraction profiles of radical species, CH, H, OH, and O. The peak mole fractions of CH and H radicals are located on the fuel side while that of O radicals is located on the oxidizer side, typical of hydrocarbon nonpremixed flames. For both the flames, the CO profile indicates an increase in CO mole fraction near $x \approx 0.4$ cm, which is due to the fact that H_2 diffuses much faster than CO.

The major difference between the two flames is the presence of CH_4 in syngas mixture for flame B. The consumption of CH_4 occurs upstream of the reaction zone (cf. Fig. 4(b)) through its conversion to CO and H_2 [4,9]. The presence of methane in syngas mixture decreases the peak flame temperature by about 120 K, and leads to the formation of a significant amount of acetylene, as indicated in Fig. 4(c). This has important implications for both NO_x and soot emissions from syngas flames, since C_2H_2 is considered to be a dominant contributor to prompt NO [4,9] as well as a major soot precursor [10,31,32].

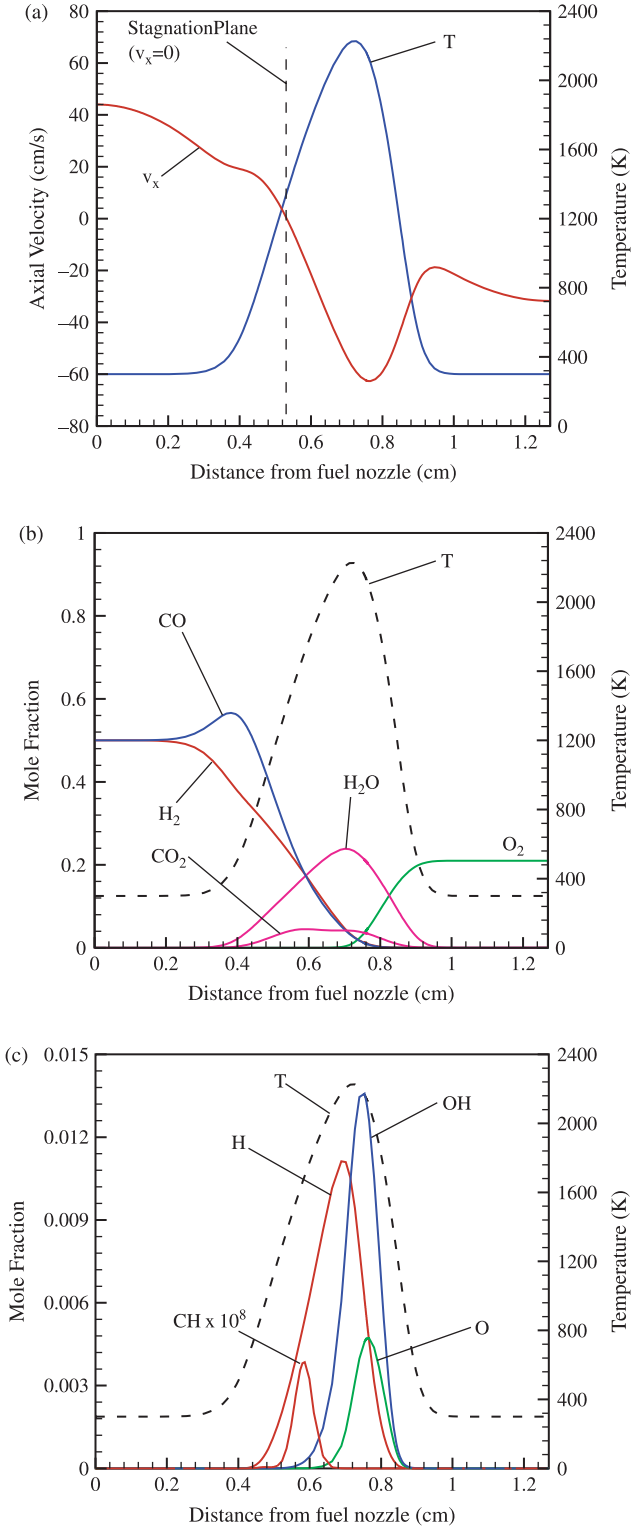

Fig. 3. The structure of flame A (50%H_2/50%CO) plotted in terms of temperature, axial velocity, and species mole fraction profiles.

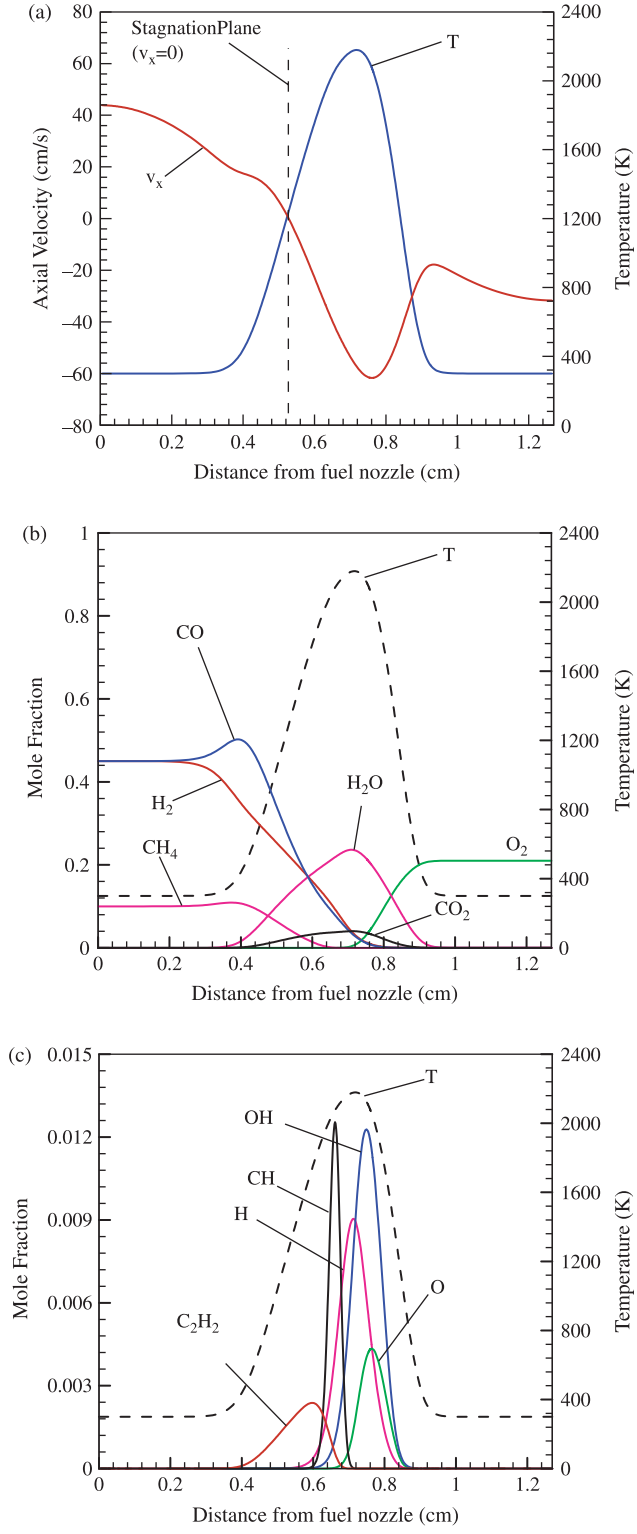

Fig. 4. The structure of flame B (45%H_2/45%CO/10%CH_4) plotted in terms of temperature, axial velocity, and species mole fraction profiles.

The comparison of NO_x characteristics of flames A and B is presented in Fig. 5, which shows the NO[1] mole fraction profiles for the two flames. The individual contributions of thermal, prompt, and N_2O-intermediate mechanisms to total NO are also shown in the figure. While the contributions of thermal and prompt mechanisms to total NO are comparable for the two flames, that of N_2O-intermediate mechanism is relatively

[1] For the conditions investigated, the contribution of NO_2 to total NO_x was found to be negligible.

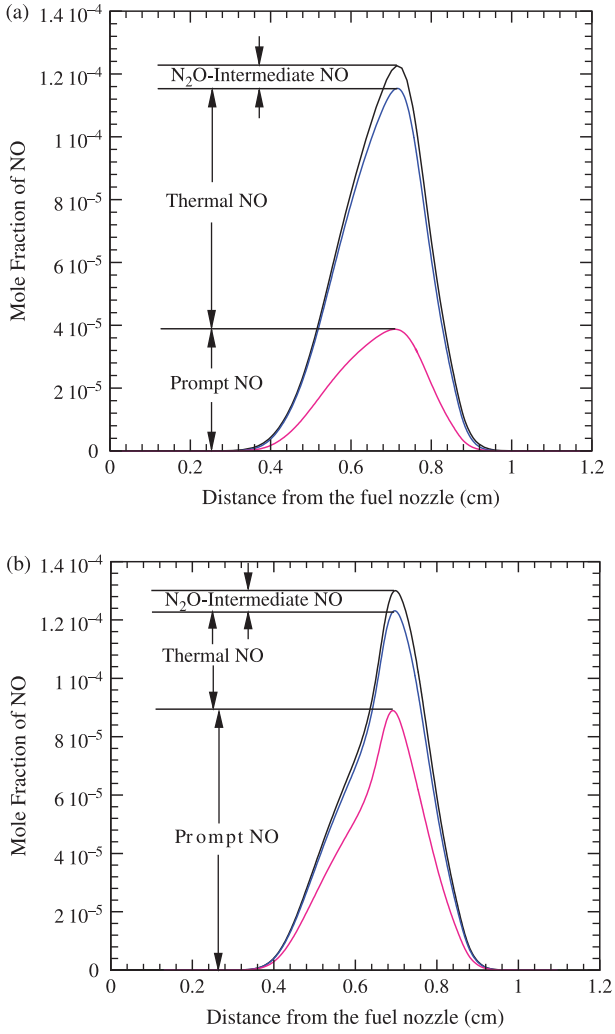

Fig. 5. NO mole fraction profile for flames A and B discussed in the context of Figs. 3 and 4. Contributions of prompt, thermal and N_2O-intermediate mechanisms to total NO are also shown.

small. This is consistent with the results of many previous studies [4,33], which have observed that the N_2O mechanism is more relevant for lean premixed hydrocarbon flames. In this context, it is also important to mention that the contribution of the NNH mechanism was found to be negligible for the nonpremixed flames investigated in the present study.

An important observation from Figs. 5(a) and (b) is that the presence of a relatively small amount of CH_4 (10 vol%) in syngas mixture not only increases the peak NO (from 122 to 130 ppm), but also leads to a significant increase in the contribution of prompt NO compared to thermal NO. This can be attributed to a large amount of acetylene formed due to the presence of methane in flame B (cf. Fig. 4(c)), which dramatically increases the formation of CH radical and thereby the formation of HCN in this flame. This is illustrated in Table 3, which lists the peak flame temperature and mole fractions of HCN, NO and important radical species. The peak values are shown for both flames A and B, and without and with the air stream dilution. For the undiluted case, the peak HCN mole fractions for flames A and B are 0.014 and 48.4 ppm, respectively, clearly highlighting the dramatic effect of the presence of methane in syngas on the formation of CH and HCN, and hence on the formation of prompt NO. As discussed in previous studies [33,34], the reaction of CH with N_2 to form HCN ($CH + N_2 \leftrightarrow HCN + N$) represents the major initiation step for the formation of prompt NO. Note that the thermal NO is reduced due to the presence of methane in syngas, since the flame temperature is reduced. However, the reduction in thermal NO is small compared to the increase in prompt NO, and, consequently, the total NO increases due to the presence of methane in syngas. It should be noted, however, that the GRI 3.0 mechanism is known to overpredict the formation of prompt NO in methane diffusion flames [4,25,29]. Consequently, the present results regarding the effect of methane on prompt NO should be considered qualitative. Nevertheless, these results indicate that the amount of NO_x formed in undiluted syngas flames is rather high, and strategies to reduce NO_x to more acceptable levels should be explored in order to meet the emission regulations for syngas combustion systems.

3.2. Effects of diluents on NO_x emissions: flame A

The relative effectiveness of N_2, H_2O, and CO_2 diluents in reducing NO_x emission in flame A (50%H_2/50%CO) is depicted in Fig. 6, which presents the NO mole fraction profiles versus the

Table 3
Comparison of peak flame temperatures and mole fractions of H, O, OH, N, HCN, and NO for flames A and B with no dilution and with 10% N_2, H_2O, and CO_2 dilution by volume

Flame	No dilution		10% N_2		10% H_2O		10% CO_2	
	A	B	A	B	A	B	A	B
T_f (K)	2226	2179	2129	2074	2120	2064	2032	1984
H (%mol fraction)	1.10	0.90	1.04	0.83	0.90	0.70	0.90	0.68
O (%mol fraction)	0.47	0.41	0.42	0.37	0.30	0.28	0.34	0.31
OH (%mol fraction)	1.35	1.22	1.13	0.98	1.12	1.02	0.95	0.83
N (ppm)	0.361	0.530	0.315	0.47	0.100	0.09	0.08	0.08
HCN (ppm)	0.014	48.4	0.009	35.0	0.005	10.0	0.004	8.0
NO (ppm)	122	130	69	87	44	57	34	48

amount of diluent added to air stream on a mole basis. As expected, for all three diluents, the peak NO mole fraction decreases as the amount of dilution is increased. On a mole basis, CO_2 appears to be the most effective agent in reducing NO, followed by H_2O, and then N_2. The relative effectiveness of each diluent is further illustrated in Fig. 7, which presents the axial profiles of temperature, and H, OH, O, N, and HCN mole fractions with no dilution and with 20% dilution by volume. The N and HCN profiles are included to indicate the effectiveness of each diluent in reducing thermal and prompt NO, respectively. Note that addition of a diluent to the air stream causes a corresponding decrease in oxygen mole fraction. Consequently, the flame temperature and the mole fractions of H, O, and OH radicals decrease for all three diluents (cf. Fig. 7(a)–(d)). The N and HCN mole fractions also decrease due to the addition of these diluents (cf. Fig. 7(e)–(f)). Even with N_2 dilution, the mole fractions of N and HCN decrease, indicating a strong effect of the reduced flame temperature and radical species (H, CH, OH, and O) concentrations on N and HCN. In general, N_2 dilution causes a smaller reduction in flame temperature and radical species concentrations compared to those with H_2O and CO_2 dilution. On a mole basis, CO_2 dilution causes a larger reduction in flame temperature compared to that with H_2O dilution, which is due to the higher specific heat of CO_2. However, on a mass basis, H_2O has a higher specific heat, and consequently, H_2O dilution would lead to a lower flame temperature. Also, on a mole basis, CO_2 dilution leads to a larger reduction in the mole fractions of OH, N, and HCN, but a smaller reduction in those of H and O, compared to H_2O dilution.

The relative effectiveness of the three diluents in reducing NO_x is summarized in Fig. 8 by plotting the peak NO mole fraction and flame temperature versus the amount of diluent added to the air stream as percent of mole (volume) and mass, respectively. Important observations are as follows:

1. All three diluents are effective in reducing NO in syngas diffusion flames, as a relatively small amount of dilution reduces the peak NO mole fraction significantly. For example, as shown in Table 3, a 10% dilution with N_2, H_2O, and CO_2 for flame A decreases the peak NO by 44, 60, and 79%, respectively. Both on mole and mass basis, H_2O and CO_2 diluents are more effective than N_2 in reducing NO emissions in syngas flames.
2. On a mole basis, H_2O dilution causes nearly the same reduction in peak flame temperature but a much larger reduction in peak NO compared to that with N_2 dilution. This implies the effectiveness of H_2O in reducing prompt NO. As discussed by Li and Williams [4], the effectiveness of H_2O in reducing prompt NO in methane–air flames is due to its chemical effect that reduces the CH concentration, and thereby the HCN concentration. This is corroborated by the HCN profiles presented in Fig. 7(f), which indicates that a 20% H_2O dilution reduces the peak HCN mole fraction by a factor of about 6, compared to a reduction by a factor of 2 with 20% N_2 dilution.
3. On a mole basis, H_2O and CO_2 cause nearly the same reduction in NO, although the flame temperature is lower

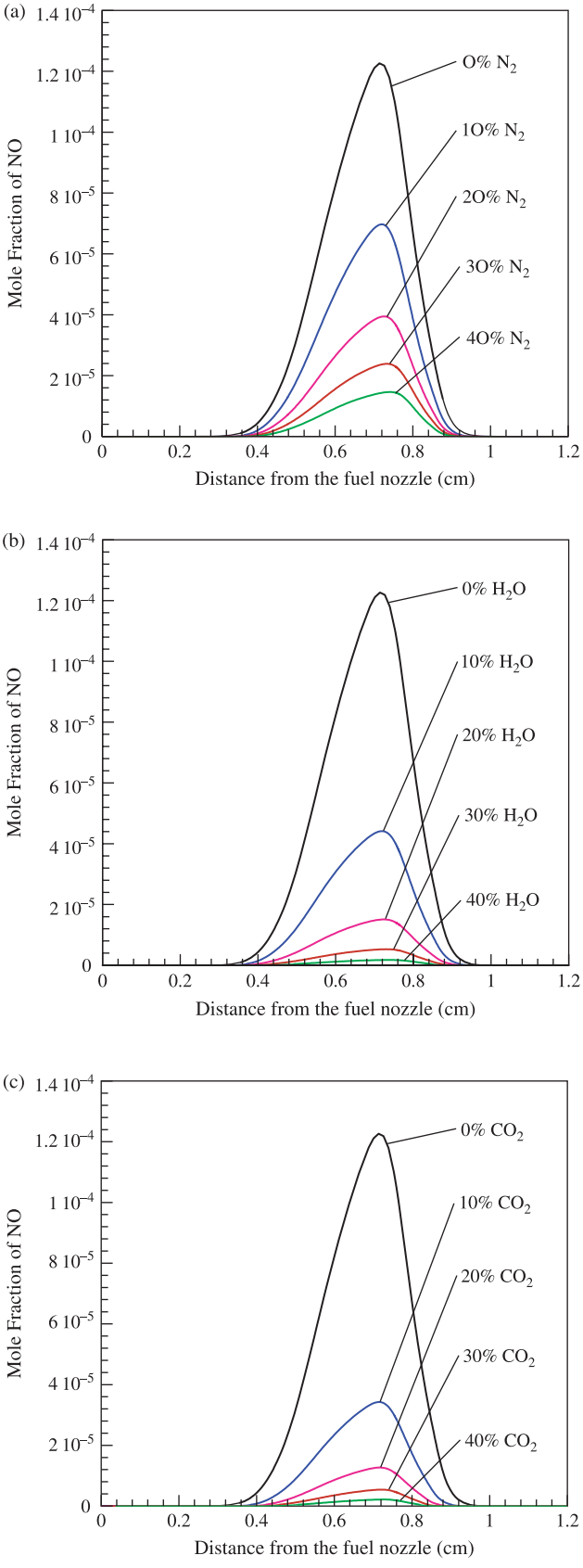

Fig. 6. Comparison of NO mole fraction profiles for flame A (50%H_2/50%CO) with different diluents in the air stream: (a) N_2; (b) H_2O and (c) CO_2.

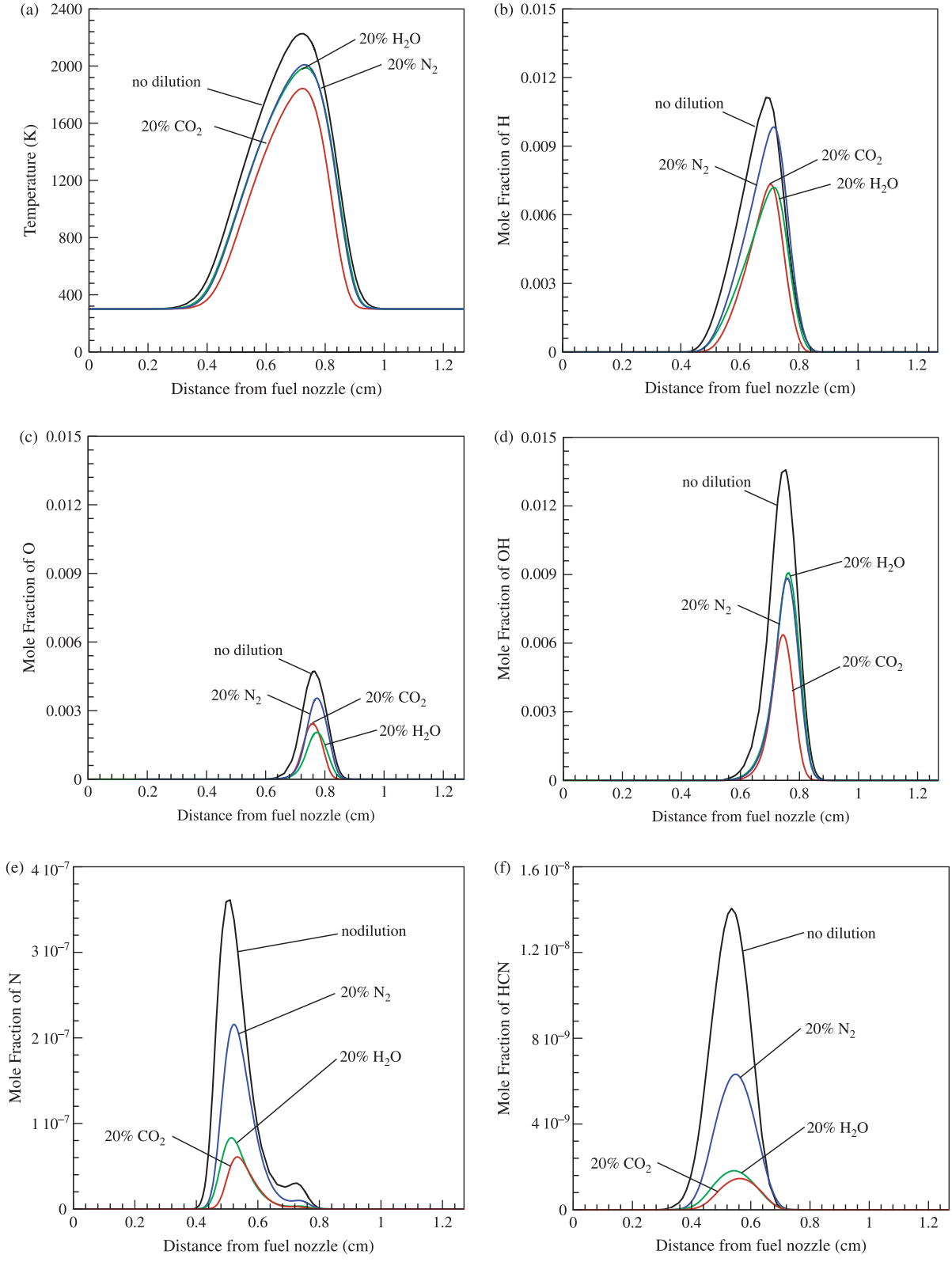

Fig. 7. Profiles of (a) temperature; (b) H; (c) OH; (d) O; (e) N and (f) HCN mole fraction for flame A with no dilution and with 20% N_2, H_2O and CO_2 dilution.

with CO_2 dilution. This can be attributed to the fact that a larger drop in flame temperature caused by CO_2 dilution is compensated by a larger drop in O radical concentration caused by H_2O dilution (cf. Fig. 7(c)).

4. On a mass basis, H_2O is the most effective diluent compared to N_2 and CO_2 in reducing both the flame temperature and NO concentration. The lower flame temperature with H_2O dilution can be attributed to its

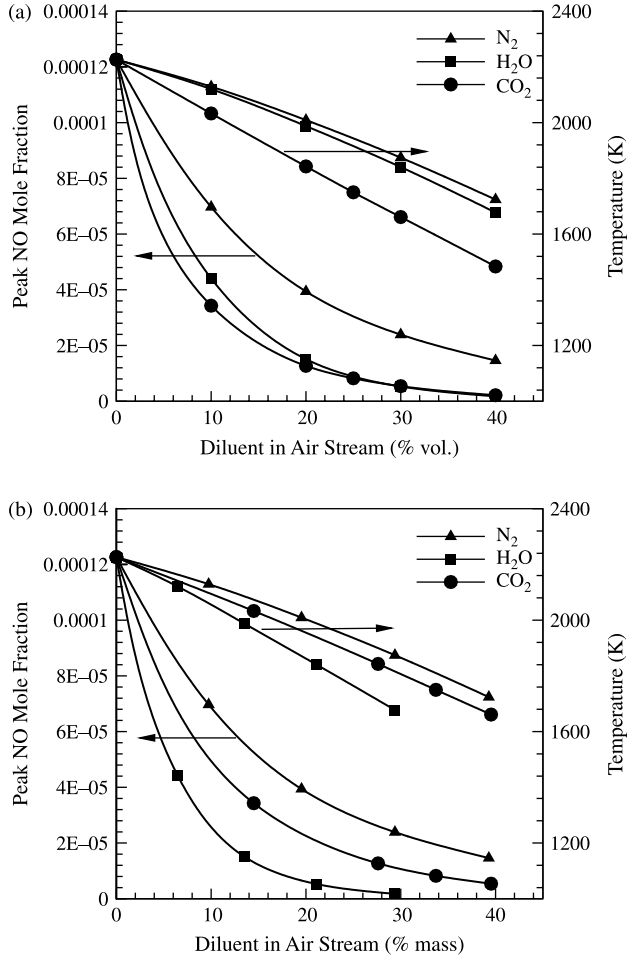

Fig. 8. Variation of peak NO mole fraction and flame temperature with the amount of diluent added to the air stream on mole (a) and mass basis; (b) for flame A.

higher specific heat, while the lower NO concentration can be attributed to both the thermal and chemical effects of H_2O dilution. The thermal effect decreases the flame temperature and thereby the thermal NO, while the chemical effect decreases the CH and HCN concentrations and thereby the prompt NO. The chemical effect of H_2O and CO_2 diluents is further depicted in Fig. 9, by plotting the peak HCN mole fraction versus the amount of diluent added by mass. A significantly larger reduction in peak HCN caused by CO_2 and H_2O compared to that by N_2 can be attributed their chemical effect.

5. The chemical effect of CO_2 and H_2O in reducing prompt NO can be inferred perhaps more clearly from Fig. 10, which presents the peak NO mole fraction as a function of the peak flame temperature. For the same peak flame temperature, H_2O dilution causes the largest reduction in NO, followed by CO_2 dilution, and then by N_2 dilution. This implies that the effectiveness of the three diluents in reducing the prompt NO and thereby the total NO can be ranked in the order $H_2O > CO_2 > N_2$. It is also important to note that at relatively high temperatures, the effectiveness of all three diluents becomes nearly the same, indicating that NO production at these temperatures is predominantly due to the thermal mechanism.

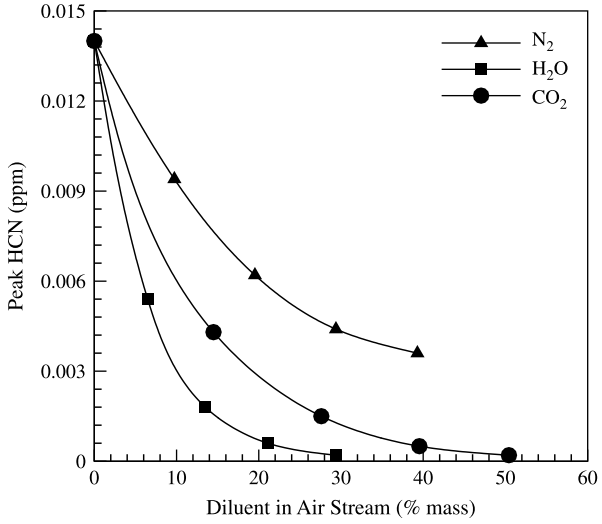

Fig. 9. Peak HCN mole fraction plotted versus the amount of N_2, H_2O and CO_2 diluents added on mass basis for flame A.

3.3. Effects of diluents on NO_x emissions in flame B

As discussed earlier, the presence of methane in syngas decreases the peak flame temperature and increases the production of prompt NO considerably, while decreasing that of thermal NO. Results are now presented to characterize the effect of methane on the effectiveness of each diluent in reducing NO_x emissions from syngas flames.

Fig. 11 presents the variation of peak NO mole fraction and flame temperature versus the amount of diluent added to air stream for flame B on both mole and mass basis. These results are qualitatively similar to those for flame A presented in Fig. 8. While all three diluents are effective in reducing the

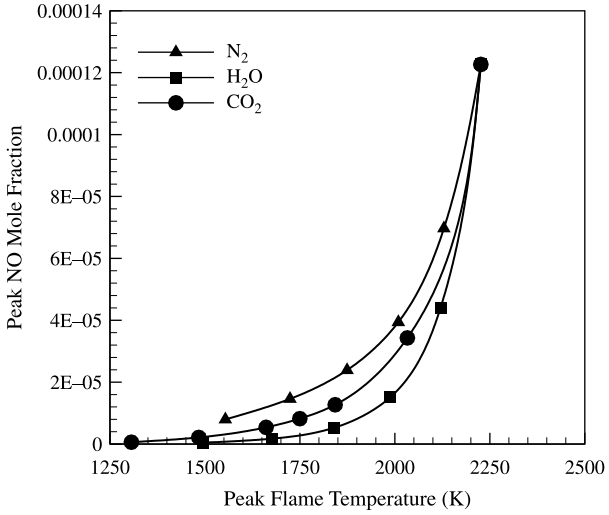

Fig. 10. Peak NO mole fraction plotted versus peak flame temperature for the three diluents discussed in the context of Fig. 8.

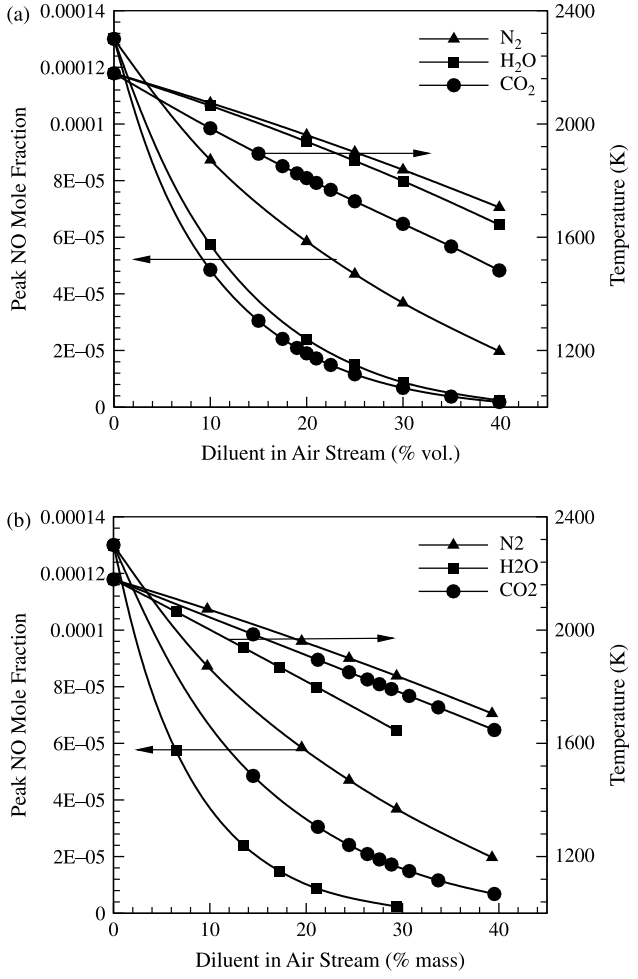

Fig. 11. Variation of peak NO mole fraction and flame temperature with the amount of diluent added on mole basis (a) and mass basis; (b) to the air stream for flame B.

peak NO considerably, CO_2 and H_2O are significantly more effective compared to N_2. On a mass basis, H_2O is more effective than N_2 and CO_2, while CO_2 is more effective than N_2, in reducing both the peak NO and flame temperature. This can again be attributed to the effectiveness of H_2O in reducing both the thermal and prompt NO, as discussed earlier in the context of flame A. In order to separate the thermal and chemical effects, the variation of peak NO mole fraction with the peak flame temperature is presented in Fig. 12. This plot is qualitatively similar to that for flame A shown in Fig. 10, indicating the effectiveness of CO_2 and H_2O relative to N_2 in reducing the production of prompt NO in both the flames.

In order to further characterize the effect of methane on diluent effectiveness, we compare in Fig. 13 the variation of peak NO mole fraction versus the amount of diluent added by mass for flames A and B. An important observation from this figure is that the presence of methane decreases the diluent effectiveness in reducing NO_x emission from syngas flames. For instance, as indicated in Table 4, a 10% dilution using N_2, CO_2 and H_2O reduces the peak NO mole fraction by 44.1, 59.7, and 79%, respectively, for flame A, and by 33.6, 49.2, and 71.4%, respectively, for flame B. The decrease in diluent

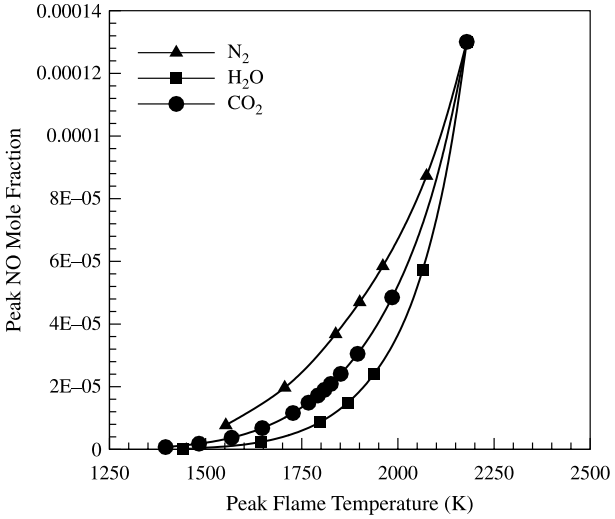

Fig. 12. Peak NO mole fraction plotted versus peak flame temperature for the three diluents discussed in the context of Fig. 11.

effectiveness can be attributed to the fact that the presence of methane causes a significant increase in the production of prompt NO in syngas flames. The increase in prompt NO can be easily inferred from the peak HCN mole fraction values for flames A and B listed in Table 3, which indicates a dramatic increase in HCN mole fraction due to the presence of methane. For instance, with 10% methane in syngas for the undiluted case, the peak HCN mole fraction increases from 0.014 to 48.4 ppm. Similar increases in peak HCN mole fractions are observed for the three diluted cases in Table 3. This dramatic increase in HCN mole fraction implies that the production of prompt NO in flame B is significantly increased. As a consequence, the diluent effectiveness is reduced due to the presence of methane in syngas.

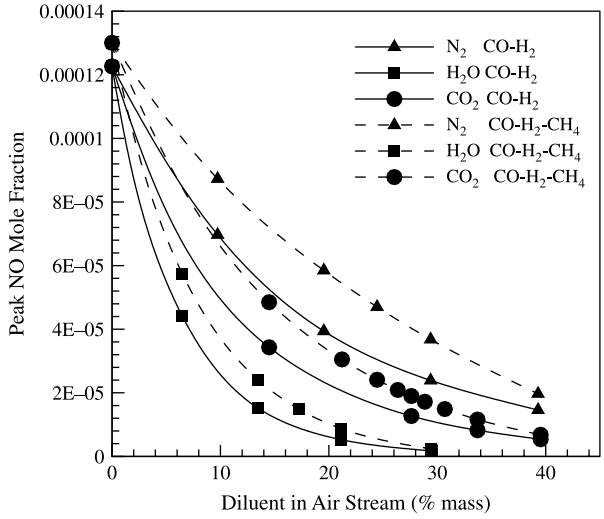

Fig. 13. Peak NO mole fraction plotted versus the amount of diluent added to the air stream by mass for flames A and B.

Table 4
Percentage reduction in peak NO and emission index ($EINO_x$) using 10% mass dilution with N_2, H_2O, and CO_2, respectively, for flames A and B

Diluent	Peak NO reduction with 10% dilution by mass		$EINO_x$ reduction with 10% dilution by mass	
	Flame A	Flame B	Flame A	Flame B
N_2 (%)	44.1	33.6	34.9	25.9
H_2O (%)	79.0	71.4	75.6	68.0
CO_2 (%)	59.7	49.2	51.8	42.0

3.4. NO_x emission index for syngas flames

The NO_x emission from syngas flames can be globally characterized using a NO_x emission index ($EINO_x$) defined as [9,35]

$$EINO_x = \frac{\int_0^L M_{NO_x}\dot{\omega}_{NO_x}\mathrm{d}x}{-\int_0^L M_{fuel}\dot{\omega}_{fuel}\mathrm{d}x} \quad (\text{g } NO_x/\text{kg fuel}) \tag{3}$$

here $\dot{\omega}$ is the production/consumption rate, M the molecular weight, and L the separation distance between the two nozzles. The emission index represents the ratio of the total NO_x production rate to the total fuel consumption rate. Since the syngas is considered a mixture of CO, H_2, and CH_4, the above equation is written as:

$$EINO_x = \frac{\int_0^L M_{NO_x}\dot{\omega}_{NO_x}\mathrm{d}x}{-\int_0^L (M_{CO}\dot{\omega}_{CO} + M_{H_2}\dot{\omega}_{H_2} + M_{CH_4}\dot{\omega}_{CH_4})\mathrm{d}x} \tag{4}$$

For flame A, the syngas contains only CO and H_2, and $EINO_x$ can be easily computed using the above equation. However, for flame B, the computation of the denominator requires additional consideration, since the fuel species CO and H_2, which represent the major components of syngas, are also produced during the oxidation of CH_4. Two cases were considered to address this issue. In the first case, only the consumption of CO and H_2 was included in calculating the denominator. This underestimated the denominator, since the methane consumption was not included, and thus over-predicted $EINO_x$. In the second case, the consumption rates of all three fuel species were included in the denominator. Since, CO and H_2 are produced from the consumption of CH_4, this overestimated the denominator and, thus, underpredicted $EINO_x$. For example, for the undiluted cases, the $EINO_x$ values predicted using these two approaches were 1.6 and 1.3 for flame B, while the corresponding value for flame A was 1.35. Since, $EINO_x$ for flame B is expected to be higher than that for flame A, based on the predicted NO concentrations for these two flames, the actual $EINO_x$ value for flame B should be between these two limiting values. In order to compare the NO_x characteristics of the two flames in terms of $EINO_x$, we used an average of the two $EINO_x$ values obtained from the two approaches for flame B.

Fig. 14 presents the variation of $EINO_x$ as a function of the amount of diluent for flames A and B. Results pertaining to the effect of diluents on $EINO_x$ for the two flames are qualitatively similar to those presented earlier in terms of the NO mole fraction plots. For both the flames, CO_2 and H_2O diluents are more effective than N_2 in reducing $EINO_x$ on a mole basis, while H_2O diluent is more effective than CO_2 and N_2 on a mass basis. The effectiveness of H_2O in reducing $EINO_x$ is again due to its high specific heat (thermal effect) and its ability to reduce the concentration of CH radicals significantly (chemical effect). The comparison of $EINO_x$ for flames A and B again indicates that the presence of methane in syngas decreases the diluent effectiveness in reducing NO_x emission from syngas flames. A comparison of the diluent effectiveness for the two flames in terms of the peak NO mole fraction and $EINO_x$ is presented in Table 4. As indicated in this table, the peak NO

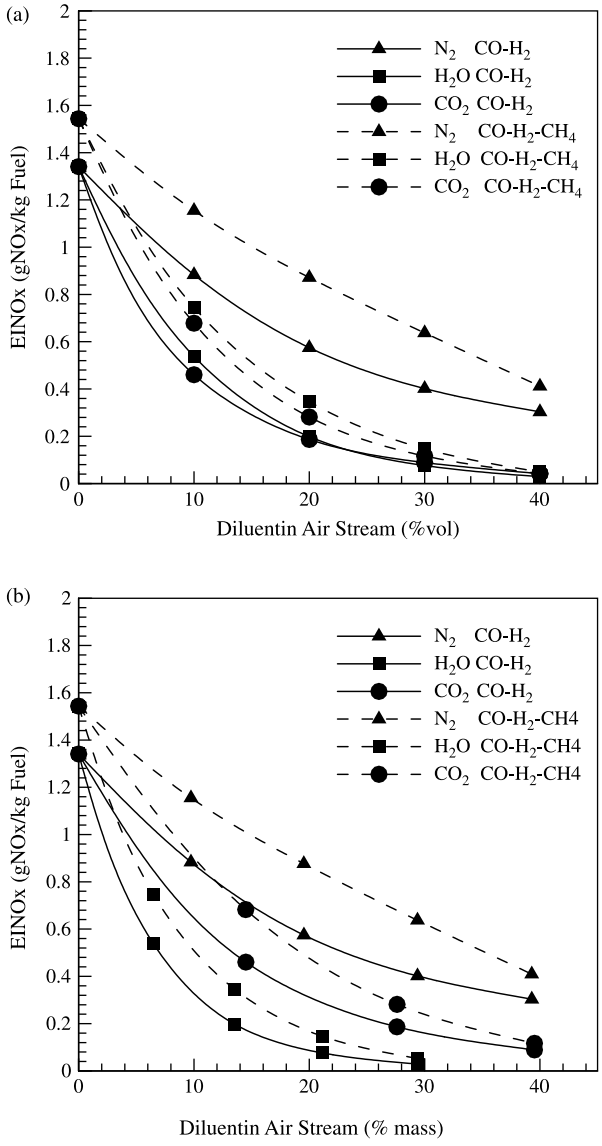

Fig. 14. Comparison of the NO_x emission index ($EINONO_x$) for flames A and B. $EINO_x$ is plotted versus the amount of diluent added on mole basis (a) and mass basis; (b) to the air stream for flames A and B.

mole fraction decreases by 44.1, 59.7, and 79.0%, respectively, with 10% N_2, CO_2, and H_2O dilution for flame A, and by 33.6, 49.2, and 71.4%, respectively, for flame B. The corresponding reductions in $EINO_x$ are 34.9, 51.8, and 75.6%, respectively, for flame A, and 25.9, 42.0, and 68.0%, respectively, for flame B.

4. Conclusions

A counterflow configuration was used to simulate syngas combustion and characterize the effects of diluents on NO_x emission in syngas nonpremixed flames. Two representative syngas mixtures, namely 50%H_2/50%CO and 45%H_2/45%CO/10%CH_4 by volume, were selected using data from various syngas power generation facilities around the world. Three diluents, namely N_2, H_2O, and CO_2, were selected based on the presence of these diluents during the gasification, refinement, and combustion of syngas. The effectiveness of these diluents was characterized in terms of their ability to reduce NO_x emissions from syngas flames. Important observations are as follows:

1. Syngas nonpremixed flames are characterized by relatively high temperatures and high NO concentrations and emission indices. The presence of methane in syngas decreases the peak flame temperature and thus the thermal NO, but increases the formation of prompt NO significantly. Consequently, for the 50%H_2/50%CO mixture, more NO is formed through the thermal mechanism compared to the prompt mechanism, while for the 45%H_2/45%CO/10%CH_4 mixture, more NO is formed through the prompt mechanism. This can be attributed to the fact that the presence of methane in syngas significantly increases the formation of acetylene, leading to a marked increase in CH concentration and thereby HCN concentration.
2. While all three diluents are generally effective in reducing NO_x emission from syngas flames, CO_2 and H_2O diluents are more effective compared to N_2. This is due to the fact that air stream dilution with CO_2 and H_2O leads to a larger reduction in both the flame temperature and the concentrations of important radical species, such as O, H, and CH.
3. On a mass basis, H_2O is a more effective diluent than both CO_2 and N_2 in reducing NO_x emissions from syngas flames. For instance, a 10% H_2O dilution decreases the peak NO concentration by 79.0% and the emission index by 75.6% in 50%H_2/50%CO syngas flame. The corresponding reductions in peak NO and $EINO_x$ are 59.7 and 51.8%, respectively, with CO_2 dilution, and 44.1 and 34.9%, respectively, with N_2 dilution. The higher effectiveness of H_2O is due to its high specific heat, which decreases the thermal NO, and its ability to reduce CH concentration that decreases the prompt NO.
4. The presence of methane in syngas reduces the effectiveness of all three diluents in reducing NO_x emissions from syngas flames. This is due the fact that the presence of methane increases the formation of acetylene considerably, which causes a significant increase in CH concentration and thereby in prompt NO. The increase in acetylene concentration also implies that soot emission is adversely affected by the presence of methane in syngas mixtures.
5. The present investigation highlights the need for experimental investigation of syngas flames in order to provide well-characterized measurements that can be used for the development and validation of simulation models. In addition, the effects of residence time and pressure on the syngas combustion and emission characteristics need to be explored in order to extrapolate the present results to gas turbines applications.

References

[1] Shilling NZ, Lee DT. IGCC—clean power generation alternative for solid fuels. Schenectady: GE Power Systems; 2003.
[2] Brdar RD, Jones RM. GE IGCC technology and experience with advanced gas turbines. Schenectady: GE Power Systems, GER-4207; 2000.
[3] Moore MJ. NO_x emission control in gas turbines for combined cycle gas turbine plant. Proc Inst Mech Eng 1997;211:43–52.
[4] Li SC, Williams FA. NO_x formation in two-stage methane–air flames. Combust Flame 1999;118:399–414.
[5] Zhao D, Yamashita H, Kitagawa K, Arai N, Furuhata T. Behavior and effect on NO_x formation of OH radical in methane–air diffusion flame with steam addition. Combust Flame 2002;130:352–60.
[6] Rortveit GJ, Hustad JE, Li SC, Williams FA. Effects of diluents on NO_x formation in hydrogen counterflow flames. Combust Flame 2002;130: 48–61.
[7] Park J, Kim S, Keel S, Noh D, Oh C, Chung D. Effect of steam addition on flame structure and NO formation in H_2–O_2–N_2 diffusion flame. Int J Energy Res 2004;28:1075–88.
[8] Rortveit GJ, Hustad JE, Williams FA. NO_x formation in diluted CH_4/H_2 counterflow diffusion flames. Proceedings of the sixth international conference on technologies and combustion for a clean environment, Porto, Portugal; 2001.
[9] Naha S, Aggarwal SK. Fuel effects on NO_x emissions in partially premixed flames. Combust Flame 2004;139:90–105.
[10] Naha S, Briones A, Aggarwal SK. Effect of fuel blends on pollutant emissions in flames. Combust Sci Technol 2005;177:183–220.
[11] Allen MT, Yetter RA, Dryer FA. High pressure studies of moist carbon monoxide/nitrous oxide kinetics. Combust Flame 1997;109:449–70.
[12] Drake MC, Blint RJ. Thermal NO_x in stretched laminar opposed-flow diffusion flames with CO/H_2/N_2 fuel. Combust Flame 1989;76:151–67.
[13] Chung SH, Williams FA. Asymptotic structure and extinction of CO–H_2 diffusion flame with reduced kinetic mechanisms. Combust Flame 1990; 82:389–410.
[14] Fotache CG, Tan Y, Sung CJ, Law CK. Ignition of CO/H_2/N_2 versus heated air in counterflow: experimental and modeling results. Combust Flame 2000;120:417–26.
[15] Charlston-Goch D, Chadwick BL, Morrison RJS, Campisi A, Thomsen DD, Laurendeau NM. Laser-induced fluorescence measurements and modeling of nitric oxide in premixed flames of CO + H_2 + CH_4 and air at high pressures. Combust Flame 2001;125:729–43.
[16] Rumminger MD, Linteris GT. Inhibition of premixed carbon monoxide–hydrogen–oxygen–nitrogen flames by iron pentacarbonyl. Combust Flame 2000;120:451–64.
[17] Natarajan J, Lieuwen T, Seitzman JM. Paper GT2005-68917, ASME-IGTI Turbo Expo, Reno, Nevada; June 6–9, 2005.
[18] Alavandi SK, Agrawal AK. Lean premixed combustion of carbon monoxide–hydrogen–methane fuel mixtures using porous inert media. Paper GT2005-68586, ASME Turbo Expo 2005, Reno, Nevada; June 6–9, 2005.

[19] Jones RM, Shilling NZ. IGCC gas turbines for refinery applications. Schenectady: GE Power Systems, GER-4219; 2003.
[20] Lutz AE, Kee RJ, Grear JF, Rupley FM. OPPDIF: A Fortran program for computing opposed flow diffusion flames. Sandia National Laboratories Report No. SAND96-8243; 1997.
[21] Kee RJ, Rupley FM, Miller JA. Chemkin: A Fortran chemical kinetics package for the analysis of gas phase chemical kinetics. Sandia National Laboratories Report No. 89-8009B; 1989.
[22] Xue H, Aggarwal SK. AIAA J 2001;39–4:637.
[23] Smith GP, Golden DM, Frenklach M, Moriarty NW, Eiteneer B, Goldenberg M, et al. GRI Mech-3.0, Available from: http://www.me.berkeley.edu/grimech/
[24] Sung CJ, Law CK, Chen JY. Proc Combust Inst 1998;27:295–304.
[25] Barlow RS, Karpetis AN, Frank JH, Chen JY. Combust Flame 2001;127:2102–18.
[26] Xue HS, Aggarwal SK, Osborne RJ, Brown TM, Pitz RW. AIAA J 2002;40(6):1236–8.
[27] Naik SV, Laurendeau NM. LIF measurements and chemical kinetic analysis of the nitric oxide formation in high pressure counterflow partially premixed and non premixed flames. Combust Sci Technol 2004;176:1809–53.
[28] Ravikrishna RV, Laurendeau NM. Laser-induced fluorescence measurements and modeling of nitric oxide in counterflow partially premixed flames. Combust Flame 2000;122:471–82.
[29] Lim J, Gore J, Viskanta R. A study of the effects of air preheat on the structure of methane/air counterflow diffusion flames. Combust Flame 2000;121:262–74.
[30] Nishioka M, Nakagawa S, Ishikawa Y, Takeno T. NO emission characteristics of methane–air double flame. Combust Flame 1994;97:127–38.
[31] Hwang JY, Lee W, Kang HG, Chung SH. Synergistic effect of ethylene–propane mixture on soot formation in laminar diffusion flames. Combust Flame 1998;114:370–80.
[32] Xu F, Lin KC, Faeth GM. Soot formation in laminar premixed methane/oxygen flames at atmospheric pressure. Combust Flame 1998;115:195–209.
[33] Xue HS, Aggarwal SK. NO_x emissions in *n*-heptane/air partially premixed flames. Combust Flame 2003;132:723–41.
[34] Miller JA, Bowman CT. Prog Energy Combust Sci 1989;15:287.
[35] Takeno T, Nishioka M. Species conservation and emission indices for flames described by similarity solutions. Combust Flame 1993;92:465–8.